

Unidirectional broadband radiation of honeycomb plasmonic antenna array with broken symmetry

Rüştü Umut Tok, Cleva Ow-Yang, and Kürşat Şendur*

*Faculty of Engineering and Natural Sciences
Sabancı University, Orhanlı - Tuzla, 34956, Istanbul, Turkey*

**sendur@sabanciuniv.edu*

Abstract: Emerging plasmonic and photovoltaic applications benefit from effective interaction between optical antennas and unidirectional incident light over a wide spectrum. Here, we propose a honeycomb array of plasmonic nanoantennas with broken symmetry to obtain a unidirectional radiation pattern over a wide spectrum. The honeycomb nanoantenna array is based on a hexagonal grid with periodically arranged nanostructure building blocks. To analyze the far-field optical distribution and spectral behavior of the plasmonic antenna honeycomb, a two-dimensional Wigner-Seitz unit cell is used together with periodic boundary conditions. As a result of the vectorial superposition of the fields produced by the Wigner-Seitz unit cells, far-zone optical fields interfere constructively or destructively in different directions. The constructive interference along the array's normal direction engenders unidirectional radiation. Due to the broken symmetry of the Wigner-Seitz cell, multiple resonances are supported by the plasmonic antenna honeycomb array over a broad spectrum.

© 2011 Optical Society of America

OCIS codes: (240.6680) Surface plasmons; (250.5403) Plasmonics.

References and links

1. P. Bharadwaj, B. Deutsch, and L. Novotny, "Optical antennas," *Adv. Opt. Photon.* **1**, 438–483 (2009).
2. L. Novotny and N. van Hulst, "Antennas for light," *Nat. Photonics* **5**, 83–90 (2011).
3. A. Hartschuh, E. J. Sanchez, X. S. Xie, and L. Novotny, "High-resolution near-field Raman microscopy of single-walled carbon nanotubes," *Phys. Rev. Lett.* **90**, 095503 (2003).
4. H. Atwater and A. Polman, "Plasmonics for improved photovoltaic devices," *Nat. Mater.* **9**, 205–213 (2010).
5. L. Wang and X. Xu, "Numerical study of optical nanolithography using nanoscale bow-tie-shaped nanoapertures," *J. Microsc.* **229**, 483–489 (2008).
6. C. Peng, "Surface-plasmon resonance of a planar lollipop near-field transducer," *Appl. Phys. Lett.* **94**, 171106 (2009).
7. K. Sendur, C. Peng, and W. Challener, "Near-field radiation from a ridge waveguide transducer in the vicinity of a solid immersion lens," *Phys. Rev. Lett.* **94**, 043901 (2005).
8. X. Gu, T. Qiu, W. Zhang, and P. K. Chu, "Light-emitting diodes enhanced by localized surface plasmon resonance," *Nanoscale Res. Lett.* **6**, 199 (2011).
9. K. A. Willets and R. P. V. Duyne, "Localized surface plasmon resonance spectroscopy and sensing," *Annu. Rev. Phys. Chem.* **58**, 267–297 (2007).
10. A. M. Gobin, M. H. Lee, N. J. Halas, W. D. James, R. A. Drezek, and J. L. West, "Near-infrared resonant nanoshells for combined optical imaging and photothermal cancer therapy," *Nano Lett.* **7**, 1929–1934 (2007).
11. N. Liu, M. L. Tang, M. Hentschel, H. Giessen, and A. P. Alivisatos, "Nanoantenna-enhanced gas sensing in a single tailored nanofocus," *Nat. Mater.* **10**, 631–636 (2011).
12. D. K. Kotter, S. D. Novack, W. D. Slafer, and P. J. Pinhero, "Theory and manufacturing processes of solar nanoantenna electromagnetic collectors," *J. Sol. Energ-T ASME* **132**, 011014 (2010).

13. T. H. Taminiau, F. D. Stefani, and N. F. van Hulst, "Enhanced directional excitation and emission of single emitters by a nano-optical Yagi-Uda antenna," *Opt. Express* **16**, 10858–10866 (2008).
14. T. Shegai, V. D. Miljkovi, K. Bao, H. Xu, P. Nordlander, P. Johansson, and M. Kall, "Unidirectional broadband light emission from supported plasmonic nanowires," *Nano Lett.* **11**, 706–711 (2011).
15. Y. G. Liu, Y. Li, and W. E. I. Sha, "Directional far-field response of a spherical nanoantenna," *Opt. Lett.* **36**, 2146–2148 (2011).
16. A. G. Curto, G. Volpe, T. H. Taminiau, M. P. Kreuzer, R. Quidant, and N. F. van Hulst, "Unidirectional emission of a quantum dot coupled to a nanoantenna," *Science* **329**, 930–933 (2010).
17. N. Bonod, A. Devilez, B. Rolly, S. Bidault, and B. Stout, "Ultracompact and unidirectional metallic antennas," *Phys. Rev. B* **82**, 115429 (2010).
18. T. Kosako, Y. Kadoya, and H. F. Hofmann, "Directional control of light by a nano-optical Yagi-Uda antenna," *Nat. Photon.* **4**, 312–315 (2010).
19. G. Vecchi, V. Giannini, and J. G. Rivas, "Shaping the fluorescent emission by lattice resonances in plasmonic crystals of nanoantennas," *Phys. Rev. Lett.* **102**, 146807 (2009).
20. A. Ahmed and R. Gordon, "Directivity enhanced raman spectroscopy using nanoantennas," *Nano Lett.* **11**, 1800–1803 (2011).
21. B. Liu, D. Wang, C. Shi, K. B. Crozier, and T. Yang, "Vertical optical antennas integrated with spiral ring gratings for large local electric field enhancement and directional radiation," *Opt. Express* **19**, 10049–10056 (2011).
22. D. Wang, T. Yang, and K. B. Crozier, "Optical antennas integrated with concentric ring gratings: electric field enhancement and directional radiation," *Opt. Express* **19**, 2148–2157 (2011).
23. X. Liu and A. Alù, "Subwavelength leaky-wave optical nanoantennas: Directive radiation from linear arrays of plasmonic nanoparticles," *Phys. Rev. B* **82**, 144305 (2010).
24. A. E. Miroshnichenko, I. S. Maksymov, A. R. Davoyan, C. Simovski, P. Belov, and Y. S. Kivsha, "An arrayed nanoantenna for broadband light emission and detection," *Phys. Status Solidi RRL* **5**, 347–349 (2011).
25. H. Aouani, O. Mahboub, E. Devaux, H. Rigneault, T. W. Ebbesen, and J. Wenger, "Plasmonic Antennas for Directional Sorting of Fluorescence Emission," *Nano Lett.* **11**, 2400–2406 (2011).
26. A. Artar, A. A. Yanik, and H. Altug, "Directional Double Fano Resonances in Plasmonic Hetero-Oligomers," *Nano Lett.* **11**, 3694–3700 (2011).
27. H. Fischer and O. J. F. Martin, "Engineering the optical response of plasmonic nanoantennas," *Opt. Express* **16**, 9144–9154 (2008).
28. E. S. Unlu, R. U. Tok, and K. Sendur, "Broadband plasmonic nanoantenna with an adjustable spectral response," *Opt. Express* **19**, 1000–1006 (2011).
29. S. V. Boriskina and L. D. Negro, "Multiple-wavelength plasmonic nanoantennas," *Opt. Lett.* **35**, 538–540 (2010).
30. C. Kittel, *Introduction to solid state physics* (Wiley, New York, NY, 2005).
31. K. Sendur, W. Challener, and C. Peng, "Ridge waveguide as a near-field aperture for high density data storage," *J. Appl. Phys.* **96**, 2743–2752 (2004).
32. J. A. Kong, *Electromagnetic wave theory* (Wiley, New York, NY, 1990).
33. C. A. Balanis, *Advanced engineering electromagnetics* (Wiley, New York, NY, 1989).
34. B. E. A. Saleh and M. C. Teich, *Fundamentals of photonics* (Wiley, New York, NY, 2007).
35. E. D. Palik, *Handbook of optical constants of solids* (Academic Press, New York, NY, 1998).
36. R. E. Collin, *Antennas and radiowave propagation* (McGraw Hill, New York, NY, 1985).
37. C. A. Balanis, *Antenna theory analysis and design* (Wiley, New York, NY, 1982).

1. Introduction

Optical nanoantennas have fascinated scientists because of their ability to manipulate light beyond the diffraction limit [1, 2]. Such an achievement at the nanoscale has enabled scientists to overcome technological barriers and expand the frontiers for scientific breakthroughs in near-field imaging [3], solar cells [4], nanolithography [5], optical data storage [6], heat assisted magnetic recording [7], light emitting devices [8], spectroscopy [9], medical applications [10], and bio-chemical sensors [11].

An essential feature of nanoplasmonic devices in emerging applications is the tailoring of far-zone radiation patterns of optical antennas, particularly their directionality. Optical antennas with unidirectional far-zone radiation patterns have important implications for photovoltaic devices, in which antennas have been utilized to improve the energy conversion efficiency [4, 12]. By embedding plasmonic particles in solar cells the absorption cross section and energy conversion efficiency have been increased [4]. One important factor that needs to be addressed to improve the performance efficiency is the mismatch between the directionality of the incident

solar radiation and the plasmonic antenna pattern. Incident solar radiation on a plasmonic solar device spans a narrow angular range. To effectively leverage the incident solar radiation, optical antennas with unidirectional patterns are essential. Since most commonly utilized nanoantennas, such as dipole and bowtie nanoantennas, have broad and uniform radiation patterns, the benefits of optical antennas with unidirectional radiation patterns are compelling much research activity [13-26].

In addition to the unidirectionality of optical antenna radiation fields, another impediment to implementing plasmonic antennas in solar cells is the spectral mismatch between the incident solar spectrum and the optical antenna spectrum. To improve the efficiency of the photovoltaic devices, optical nanoantennas should be operational in the spectral region where the majority of solar energy is present and the absorption efficiency of semiconductor devices is low [4]. However, the spectrum of incident solar radiation is broad, while the spectrum of plasmonic nanostructures is narrow with sharp resonances [27]. There is an emerging need for plasmonic nanoantennas operating over a broad spectral regime that conforms with low absorption regions of photovoltaic devices [28,29].

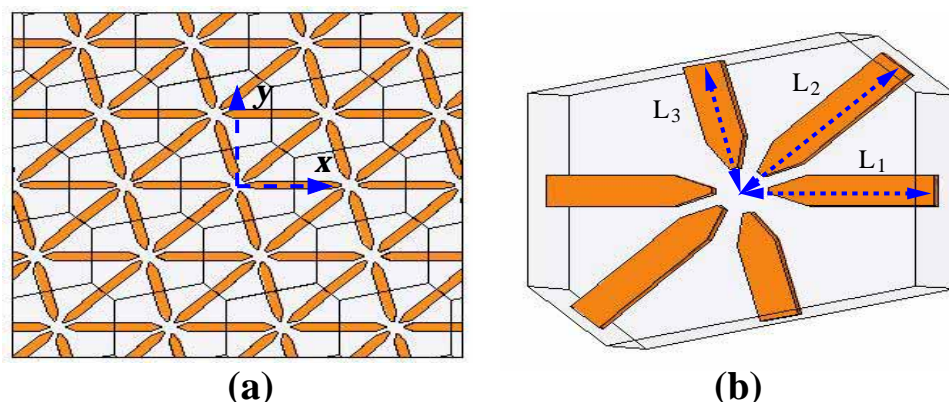


Fig. 1. (a) A schematic illustration of the honeycomb plasmonic nanoantenna array. The boundaries of Wigner-Seitz cells are highlighted with thin-black lines.(b) An asymmetric Wigner-Seitz unit cell which forms the building block of the honeycomb plasmonic nanoantenna array.

To address the need for a unidirectional antenna pattern with a wide spectral response, we propose a honeycomb array of plasmonic nanoantennas with broken symmetry. As illustrated in Fig. 1(a), the honeycomb nanoantenna is composed of periodically arranged nanostructures distributed over a hexagonal grid. The honeycomb array of plasmonic nanoantennas is a surface plasmon device with two dimensional Wigner-Seitz unit cells [30] as the building blocks. As we demonstrate in this work, the surface plasmon device shows a substantially different radiation pattern than its constituents in terms of unidirectionality. The gap formed at the convergence point of the nanoparticles serves as the lattice point for the Wigner-Seitz unit cell. To analyze the far-field optical distribution and spectral behavior of the honeycomb plasmonic antenna, periodic boundary conditions are applied to the Wigner-Seitz unit cell. The plasmonic antenna honeycomb array is investigated in symmetric and asymmetric configurations. First, the antenna honeycomb is analyzed in a symmetric configuration to demonstrate the unidirectional radiation pattern of the structure. In the second part, the symmetry of the Wigner-Seitz unit cell is broken to obtain wide spectral radiation from the antenna array.

2. Methodology

To analyze the problems in this study, a two-step procedure is used. In the first step, near-field distributions are obtained using a full-wave solution of Maxwell's equations. Once the near-zone field distribution is obtained, the far-zone pattern is obtained in the second step by propagating the near-zone fields to the far-zone using Huygen's principle. Near-field distributions are obtained using a 3-D frequency-domain finite element method [7, 31]. The accuracy of the solution technique was previously validated by comparison with other solution techniques [7, 31]. In the solution procedure, the near-zone total electric field $\vec{E}^{\text{NF}}(\vec{r})$ is defined as the summation of two components, $\vec{E}^i(\vec{r})$ and $\vec{E}^s(\vec{r})$. The incident field $\vec{E}^i(\vec{r})$ represents the optical beam in the absence of the nanoantenna. The nanoantennas are excited by a Hertzian dipole placed within the antenna gap. Once the fields generated with the Hertzian dipole interact with the nanoantenna, a scattered field $\vec{E}^s(\vec{r})$ is generated. To obtain the scattered field $\vec{E}^s(\vec{r})$, we used a full-wave solution of Maxwell's equations based on the 3-D finite element method (FEM). Two different types of boundary conditions are implemented for the different problems addressed in this study. For the isolated nanoantenna, the simulation domain is cubical with the medium surrounding the antenna chosen to be vacuum, and radiation boundary conditions are used on the cubical boundaries. For the analysis of the nanoantenna array, periodic boundary conditions are used to reduce the computational time and memory demands. This boundary condition mimics the periodic nature of the nanoantenna array, by analyzing a single Wigner-Seitz cell, rather than by analyzing a layer containing large numbers of repeating antenna geometries. To account for the presence of neighboring unit cells, three master/slave boundary conditions are defined on the three mutual, face-to-face lateral surfaces of the hexagonal shaped Wigner-Seitz unit cell, as shown in Fig. 1(b). On the top and bottom surfaces of the unit cell, radiation boundary conditions are used. In the solution procedure tetrahedral elements are used to discretize the computational domain, which accurately represents the scattering geometries used in this study. On the tetrahedral elements, edge basis functions and second-order interpolation functions are used to expand the field distributions. Adaptive mesh refinement is used to improve the coarse solution regions with high field intensities and large field gradients. Once the scattered field is solved via FEM, the total near-zone electric field distribution $\vec{E}^{\text{NF}}(\vec{r})$ is obtained by adding the incident field to the scattered field.

Once the near-zone field distribution $\vec{E}^{\text{NF}}(\vec{r})$ is obtained, the far-zone field distribution $\vec{E}^{\text{FF}}(\vec{r})$ was determined by using the radiation integrals described by Huygen's principle [32, 33]. In this problem, the field distribution in the upper semi-infinite space is of interest for determining the antenna radiation pattern. Huygen's principle states that the electromagnetic fields in a region of space, which in our case is the upper semi-infinite space, can be obtained by radiating the near-zone electric field over the enclosed surfaces [32, 33]. By using the far-zone approximations, the field distribution in the far-zone can be expressed in terms of the near-zone field as

$$\vec{E}^{\text{FF}}(\vec{r}) = i\omega\mu \left[I + \frac{1}{k^2} \nabla \nabla \right] \cdot \frac{\exp(ikr)}{4\pi r} \int_{-\infty}^{\infty} \int_{-\infty}^{\infty} dS' \exp(-i\vec{k} \cdot \vec{r}') \left(2\vec{E}^{\text{NF}}(\vec{r}') \times \hat{z} \right) \quad (1)$$

In this expression, \vec{E}^{FF} represents the far-zone electric field, \vec{E}^{NF} is the field at a distance of 1 nm from the antenna, and k is the wavenumber. It is worth emphasizing that the integral in Eq. (1) relates the near-zone and far-zone fields as Fourier Transform pairs of one another [34].

3. Results

The far-zone radiation of a single isolated optical nanoantenna is determined by the antenna geometry, its material properties, and the excitation properties including wavelength and polarization, the effects of which have been extensively studied in the literature [1, 2]. The ability to

tailor far-zone optical patterns and obtain directional antennas with a narrow radiation pattern is limited when using an isolated optical nanoantenna due to its spatially constrained near-zone distribution. This constraint is a result of an immediate corollary of Huygen's principle, which states that near-field and far-field distributions are Fourier transformation pairs [34]. This indicates that a limited distribution in the near-field leads to a broad and uniform distribution in the far-field.

To illustrate the far-field limitations of isolated optical nanoantennas, we used a single, symmetric snowflake antenna, which is composed of six identical particles around a common gap [28]. This structure radiates in the absence of other nanoantennas, thus providing a benchmark for comparison with the other results in the manuscript. Gold is chosen as the nanoantenna material due to its strong plasmonic characteristics and its resistance to corrosion. The dielectric constant of gold is taken from the experimental data by Palik [35]. The length of each nanoantenna arm is 100 nm. The thickness and width of the antenna are both 20 nm, and the gap is 30 nm. Figure 2 demonstrates the near-zone field distribution and far-zone radiation pattern of a single symmetric snowflake antenna. The field distribution in Fig. 2(a) demonstrates the near-field solution, which is plotted on a cut-plane 1 nm above the antenna. The antenna is excited by a Hertzian dipole oriented in the \hat{x} -direction, which is placed within the antenna gap. The excitation wavelength is set at 725 nm, which is the resonance wavelength of a symmetric snowflake antenna with arm length 100 nm, as shown in Fig. 2(b). Using the near-zone field in

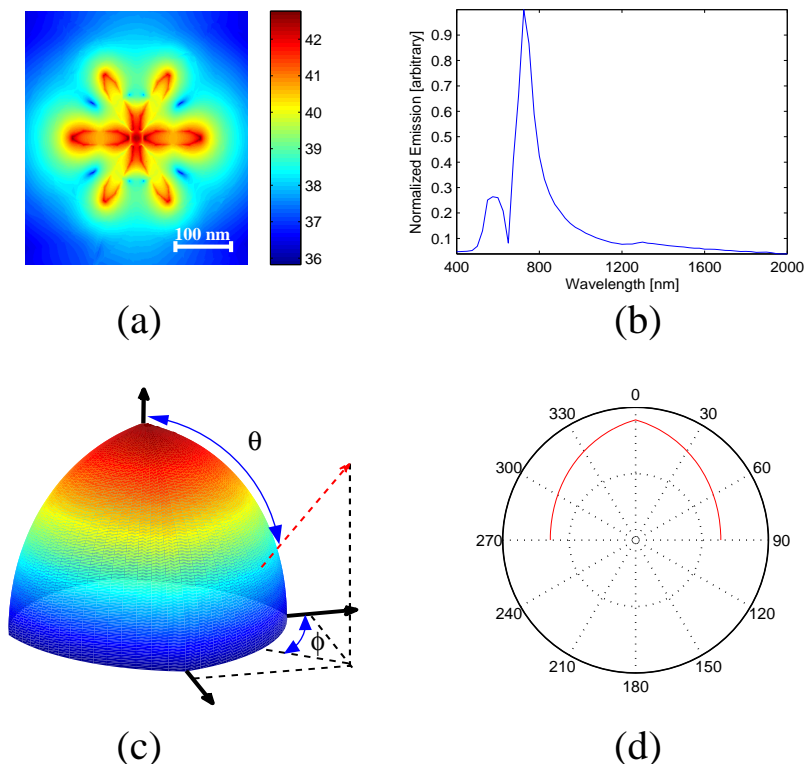


Fig. 2. (a) Near-zone field distribution for the isolated antenna plotted on the plane 1 nm above the antenna; (b) Spectral distribution of the antenna far-field radiation in the normal direction; (c) Far-zone radiation pattern for the isolated antenna; and (d) Far-zone radiation pattern for the isolated antenna on $\phi = 0^\circ$ cut.

Eq. (1), the far-zone radiation pattern is obtained. As shown in Fig. 2(c) and (d) the far-zone distribution is fairly uniform in all directions, i.e. an isolated optical antenna radiates without substantial directionality. The ability to engineer the far-zone pattern via single optical antennas is constrained and tailoring the unidirectionality of a single emitter via the geometric, material, and excitation related parameters is limited.

To achieve the desired far-zone optical patterns and directionality more effectively, a large number of the optical nanoantennas are arranged in a honeycomb configuration to form an antenna array. Such antenna arrays have been widely used to obtain directional radiation for microwave and radio frequency (RF) applications [36, 37]. The array parameters, such as the distance between the antenna elements and amplitude of the array elements, can be adjusted to tailor the far-zone optical patterns and directionality. Recent studies also extend the array pattern concept to plasmonic antennas [19] and plasmonic nanoparticles on a rectangular array [15].

To tailor the radiation pattern and obtain a unidirectional radiating antenna, the honeycomb plasmonic antenna array shown in Fig. 1 is investigated. Figures 3(a) and (b) show the resulting near-field distribution over the honeycomb plasmonic antenna array and the distribution over a single Wigner-Seitz cell, respectively. The antenna array is excited using Hertzian dipole excitations oriented in the \hat{x} -direction. The thickness and width of the antenna are both 20 nm,

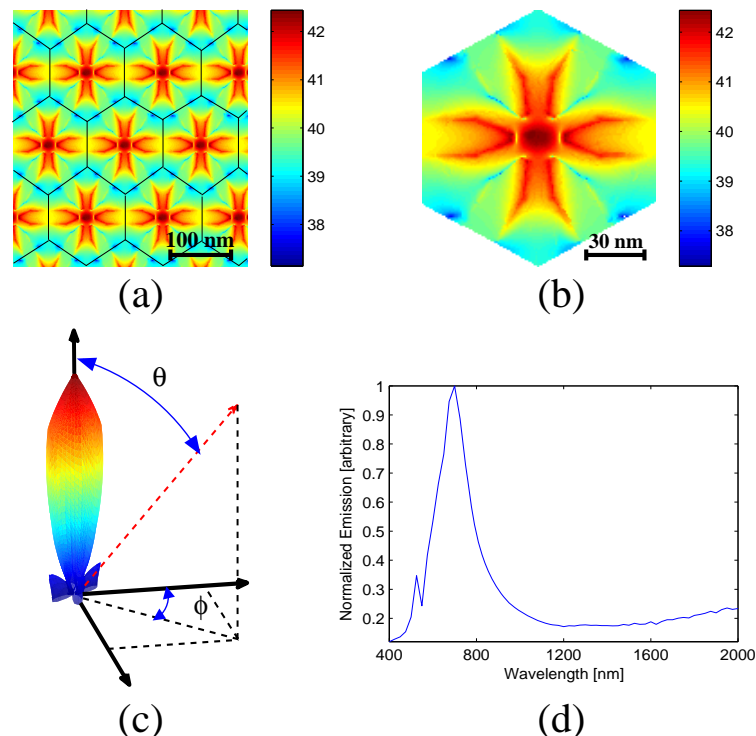


Fig. 3. (a) Near-zone field distribution for the honeycomb plasmonic antenna array plotted on the plane 1 nm above the antenna. The boundaries of Wigner-Seitz cells are highlighted with thin-black lines. (b) Near-zone field distribution on a single Wigner-Seitz unit cell of the honeycomb plasmonic antenna array; (c) Far-zone radiation pattern for the honeycomb plasmonic antenna array; and (d) Spectral distribution of the antenna far-field radiation in the normal direction for the honeycomb plasmonic antenna array.

and the gap is 30 nm. The unit cell dimensions are $L_1 = L_2 = L_3 = 65$ nm. The antenna is operated at $\lambda = 700$ nm, which corresponds to the resonance wavelength as shown in Fig. 3(d). In Figs. 3 and 4 the corresponding number of unit cells is 121. The far-zone field distribution of the symmetric plasmonic antenna honeycomb is shown in Fig. 3(c). A comparison of the far-zone radiation of an isolated antenna and the honeycomb antenna array is presented in Fig. 4. The far-zone response of the isolated antenna in Fig. 4 is multiplied by 30 so it can be compared on the same scale as the antenna array. The results demonstrate that the radiation pattern of the honeycomb plasmonic antenna array gains directionality.

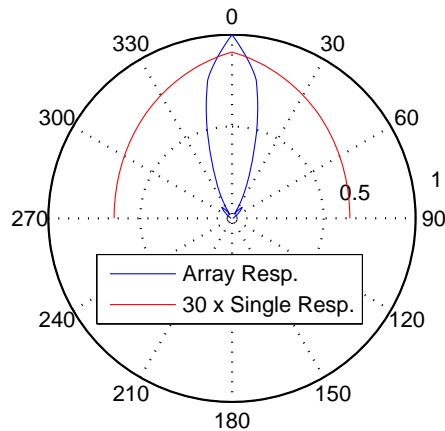


Fig. 4. A comparison between the far-zone radiation pattern of the honeycomb plasmonic antenna array and the isolated nanoantenna on $\phi = 0^\circ$ cut.

The optical field of a honeycomb plasmonic antenna array is a vectorial superposition of the fields produced by the individual antenna elements defined by the Wigner-Seitz unit cell. By adjusting the size of the Wigner-Seitz unit cell as well as the relative amplitude of each cell, the far-zone optical fields can be induced to interfere constructively or destructively at different directions. As the results in Figs. 3 and 4 suggest, the optical fields produced by the honeycomb plasmonic antenna array interact constructively along the normal direction. As illustrated in Figs. 1 and 3(a), the individual Wigner-Seitz cell geometries and near-zone field distributions over these cells are identical. When the nanoantennas are in phase, their optical fields add in the $\theta = 0$ direction. As the observation angle θ increases, the fields destructively interfere with each other, creating directions of dark radiation. As θ further increases, the fields produced by individual antennas constructively interfere again, creating local maxima. These local maxima, or side-lobes, are much weaker than the maxima in the $\theta = 0$ direction. As θ increases, dark and bright radiation patterns repeat. At $\theta = \pm\pi/2$, the fields destructively interfere as shown in Figs. 3 and 4.

The unidirectional radiation pattern of a honeycomb plasmonic antenna array can be further understood by classical antenna theory [36, 37], which states that the radiation pattern of an antenna array can be calculated by multiplying the radiation pattern of an individual antenna pattern, or element factor, with the array factor quantity. The array factor relates the effects of various array parameters, such as the position of the antenna array elements and their amplitude, to the radiation pattern of the entire array. By applying classical antenna theory [36, 37], the radiation pattern of a honeycomb plasmonic antenna array can be calculated as

$$R(\theta, \phi) = Y(\theta, \phi) \times AF(\theta, \phi) \quad (2)$$

where $R(\theta, \phi)$ is the radiation pattern of the honeycomb plasmonic antenna array, $Y(\theta, \phi)$ is the pattern of the individual antenna element defined by the Wigner-Seitz unit cell, and $AF(\theta, \phi)$ is the array factor in classical antenna theory, which is given as

$$AF(\theta, \phi) = \sum_{m=-N}^N \sum_{n=-N}^N \exp(-i\vec{k} \cdot \vec{r}_{mn}) \quad (3)$$

for an array with equal amplitude and phase. In Eq. (3), \vec{r}_{mn} is the location of the Wigner-Seitz cell center, which corresponds to the gap center of the antenna and the wavevector is $\vec{k} = k_x\hat{x} + k_y\hat{y} + k_z\hat{z}$. By using the geometric parameters associated with the honeycomb plasmonic antenna array and the Wigner-Seitz unit cell, the array factor formula can be simplified. The geometric parameters are illustrated in Fig. 5. Every gap center in the honeycomb array element represents a lattice point, so each point can be represented as a linear combination of primitive translation vectors given as

$$\vec{r}_{mn} = m\vec{a} + n\vec{b} \quad (4)$$

where m and n are integers. Each antenna in the array is identified with indices m and n , where m and n represent the individual antenna's order within the antenna array in the \vec{a} and \vec{b} directions, respectively. The indices m and n are bounded by $-N \leq m \leq N$ and $-N \leq n \leq N$. For a given N , the number of unit cells in the honeycomb antenna array is $(2N + 1) * (2N + 1)$. The lengths of the lattice vectors are $|\vec{a}| = 2L_1$ and $|\vec{b}| = 2L_2$. The lattice vector in Eq. (4) can be represented as

$$\vec{r}_{mn} = 2mL_1\hat{x} + 2nL_2(\cos\alpha\hat{x} + \sin\alpha\hat{y}) \quad (5)$$

By substituting Eq. (5) into Eq. (3) for an array of $(2N + 1) * (2N + 1)$, we obtain

$$AF(\theta, \phi) = \left| \frac{\sin((2N + 1)k_xL_1)}{\sin(k_xL_1)} \right| \left| \frac{\sin((2N + 1)[\cos\alpha k_xL_2 + \sin\alpha k_yL_2])}{\sin([\cos\alpha k_xL_2 + \sin\alpha k_yL_2])} \right| \quad (6)$$

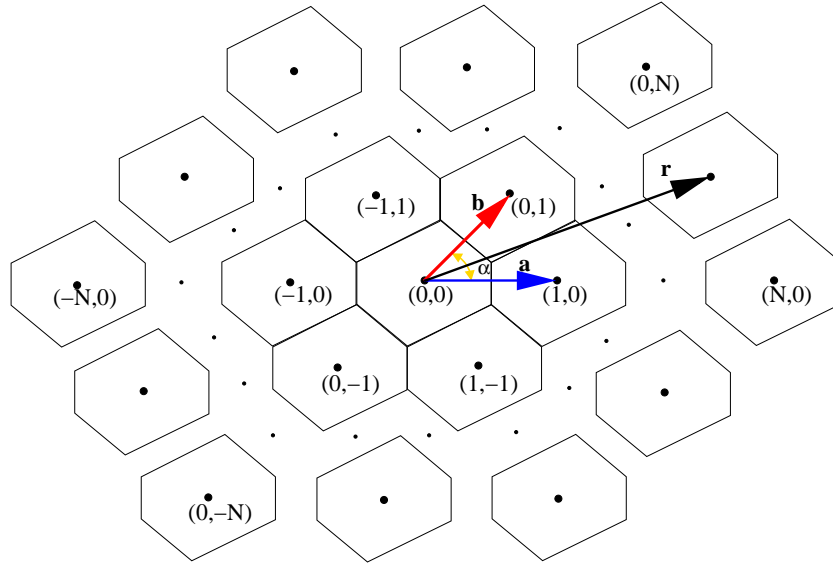


Fig. 5. A schematic representation of the geometric parameters associated with a honeycomb plasmonic antenna array that are used in the array pattern calculation.

Equation (2), Eq. (3), and Eq. (6) state that the radiation of an antenna array is the superposition of individual antenna elements. Equation (6) represents the array factor for the case of a honeycomb array of plasmonic nanoantennas with broken symmetry, which becomes symmetric when $|\vec{a}|=|\vec{b}|$ and $\alpha = 60^\circ$. Figs. 6(a) and (b) illustrate the individual antenna element pattern $Y(\theta, \phi)$ and the array pattern $AF(\theta, \phi)$. In Fig. 6(b) the corresponding number of unit cells is 121. By comparing the results in Fig. 6 with those in Figs. 3 and 4, it is clear that the unidirectionality is dominated by the array factor $AF(\theta, \phi)$. In other words, the individual building blocks of the honeycomb array radiate without substantial directionality, whereas the honeycomb arrangement of such structures operates as a unidirectional radiator. The array factor in Eq. (6) mathematically describes the interaction of the antenna elements with each other which results in an interference pattern. The array factor in Eq. (6) takes into account that the radiated waves from individual antennas interfere and interact constructively in certain directions and destructively in others, generating the pattern formations shown in Figs. 3, 4, and 6.

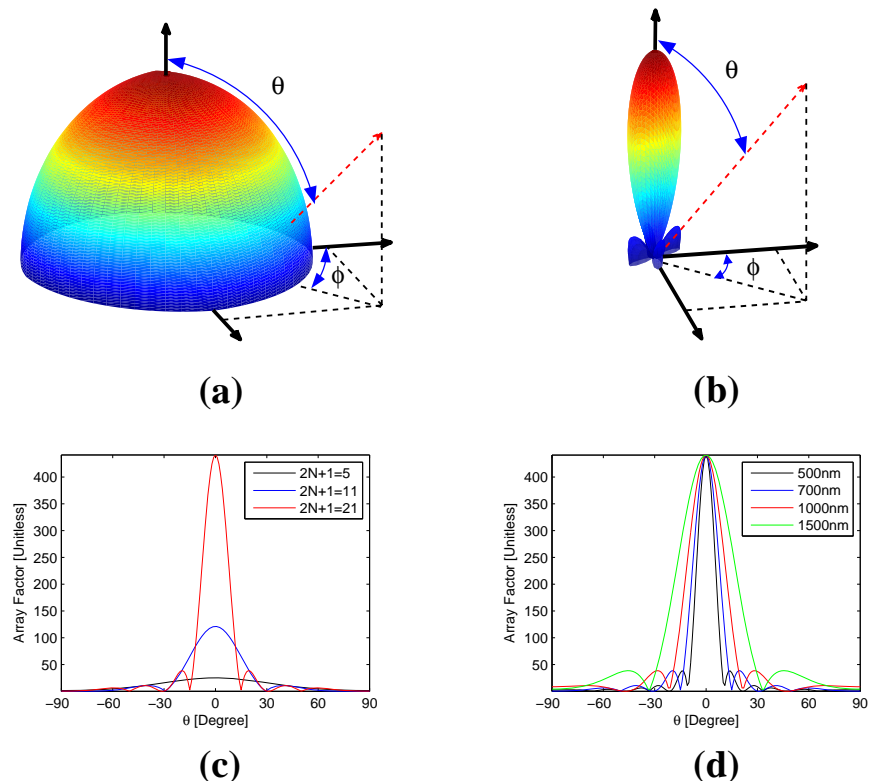


Fig. 6. (a) Individual antenna element pattern $Y(\theta, \phi)$ for the honeycomb plasmonic antenna array; (b) The array pattern $AF(\theta, \phi)$ for the honeycomb plasmonic antenna array; (c) The effect of the increased number of array elements on the directionality of the radiation pattern; and (d) The effect of the wavelength on the directionality of the radiation pattern.

As the number of elements in the plasmonic antenna honeycomb array increases, the radiation from the antenna becomes increasingly unidirectional. Figure 6(c) illustrates the effect of the increased number of array elements on the antenna radiation pattern. In Fig. 6(c) the

array pattern is compared for 25, 121, and 441 hexagonal unit cells. With increasing sources of radiation related through a fixed spatial frequency, the interference becomes stronger. The dominant main lobe of radiation is a result of the constructive interference between all of the array elements, directing stronger radiation in the normal direction. The path difference between the antenna elements creates more constructive and destructive interferences, which generate a larger number of lobes and a narrower main lobe for a plasmonic antenna honeycomb array as the number of array elements increase. These physical interpretations are supported by Eq. (6). As the number of elements increases, the oscillations due to the $(2N + 1)$ factor in the $\sin(\cdot)$ term in the nominator increases, which causes the number of lobes to increase and the width of the main lobe to decrease. As shown in Fig. 6, the array factor is the dominant contributor to the far-field distribution. As the array pattern demonstrates, the far-field distribution becomes more directional as the number of antenna elements increases. The results demonstrate that the array factor determines the directionality of the honeycomb plasmonic antenna array, whereas the small variations in the individual cells do not cause major differences in the far-field directionality.

The directionality of the honeycomb plasmonic antenna array as a function of wavelength is also studied. The results in Fig. 6(d) suggest that the antenna is more directional for shorter wavelengths. The radiation from the honeycomb plasmonic antenna array becomes broader as the wavelength increases. The narrow radiation pattern can be attributed to the electrical size of the structure as the wavelength is changed. The physical size of the honeycomb array is the same for all cases, since the number of array elements and the size of the Wigner-Seitz cells are the same. This results in a larger electrical size for shorter wavelengths. Therefore, a more narrow distribution in the far-field is obtained for shorter wavelengths due to the duality of the Fourier Transformation: a broader distribution space domain leads to a narrower spectral domain.

By breaking the symmetry of the Wigner-Seitz unit cell, broader spectral radiation is obtained from the plasmonic antenna honeycomb array. Figure 7 illustrates the peak radiation from the honeycomb plasmonic antenna array in the far-field for various asymmetric Wigner-Seitz cell sizes as listed in Table 1. The antenna array is excited using Hertzian dipole excitations oriented in the \hat{x} -direction. The thickness and width of the antennas are both 20 nm, and the gap is 30 nm. In the antenna array 121 unit cells are used. The spectral distributions of the far-field radiation for different cases underscore the wide spectral response for asymmetric antennas, as shown in Fig. 7. This can be attributed to the multiple resonances supported by the entire

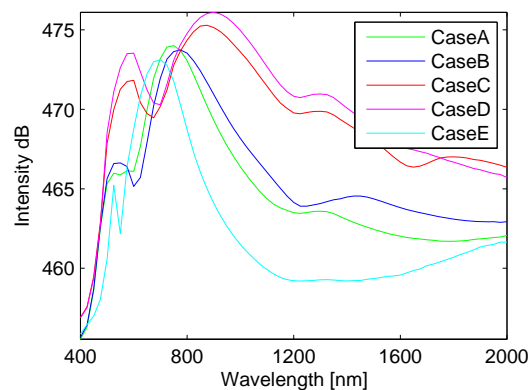


Fig. 7. Spectral distribution of antenna far-field radiation in the normal direction for various asymmetric honeycomb plasmonic antenna arrays with dimensions listed in Table 1.

Table 1. A list of Wigner-Seitz cell dimensions used in this study.

Case ID	L_1 [nm]	L_2 [nm]	L_3 [nm]
Case A	75	85	65
Case B	80	95	65
Case C	95	115	75
Case D	100	115	85
Case E	65	65	65

structure. The broken symmetry of the Wigner-Seitz cell stems from the plasmonic antenna honeycomb, consisting of antenna arrays with different dimensions that are aligned in three different directions. As a result of different particle dimensions, multiple resonances arise. The length variations between particles within the Wigner-Seitz cell are not large. As a result, although the overall structure displays multiple resonance behavior, those resonances combine to form a broadband spectral response as shown in Fig. 7. Due to the coupling of the antennas, the bandwidth is broader for the antenna array compared to the isolated antenna. The spectral peak for the symmetric array case shows a small blue shift of 25 nm. The shift is small due to the perfect symmetry in all six directions. However, when a slight asymmetry is introduced, the antenna array shows a substantial shift in the spectral peak as shown in Fig. 7. Within a

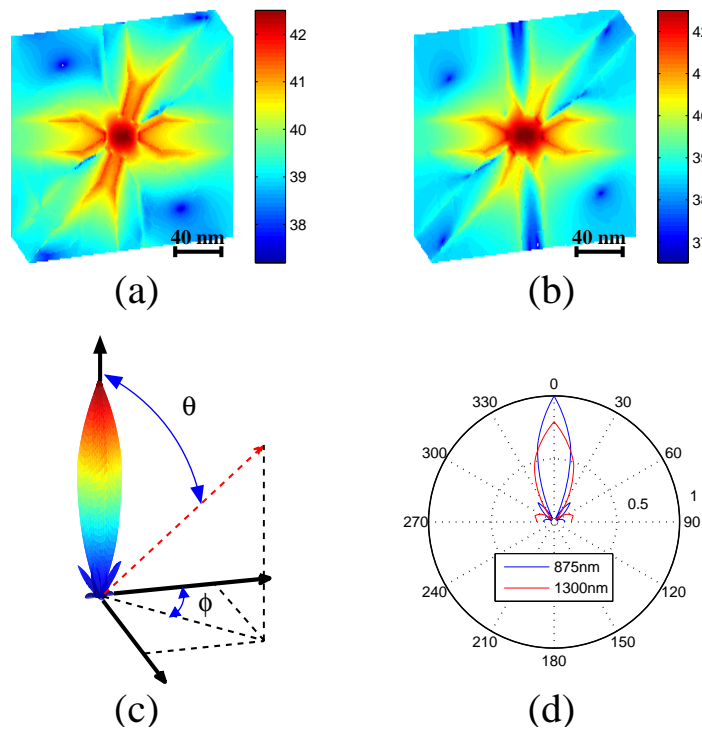


Fig. 8. (a) The near-zone field distribution of an asymmetric single Wigner-Seitz unit cell in the honeycomb plasmonic antenna array at $\lambda=875$ nm; (b) the near-zone field distribution at $\lambda=1300$ nm; (c) The far-zone radiation pattern for the asymmetric honeycomb plasmonic antenna array at $\lambda=875$ nm; (d) A comparison of the far-zone radiation pattern of the asymmetric honeycomb plasmonic antenna array at different spectral peaks.

unit cell, when one basis vector is longer than the other, the length variation between antenna pairs becomes larger, increasing the separation between spectral peaks of the antennas. If one or two sides of the unit cell becomes longer, i.e. when planar rotational symmetry is broken, the antenna array becomes more directional, skewing toward the direction of the longer antenna side as predicted by Eq. (6). A similar effect on the directionality is also obtained if the number of array elements on one side is increased.

The near-zone field distribution and far-zone radiation patterns of the asymmetric antenna with the geometric parameters corresponding to Case C are presented in Fig. 8. In the antenna array 121 unit cells are used. The results demonstrate that the far-zone radiation pattern is unidirectional for an asymmetric honeycomb plasmonic antenna array, similar to the symmetric case. As the far-zone results in Fig. 8(d) demonstrate, the antenna preserves directionality at different frequencies, although the antenna array is more directional at shorter wavelengths.

4. Conclusion

In summary, a unidirectional radiation pattern over a wide spectrum was obtained using a honeycomb plasmonic antenna array with broken symmetry. Isolated antennas radiated without substantial directionality. By periodically arranging the antennas as two dimensional Wigner-Seitz unit cells over a hexagonal grid, unidirectional radiation was achieved in the normal direction due to constructive interference of individual elements. The honeycomb array of plasmonic nanoantennas shows a substantially different radiation pattern than its constituents in terms of unidirectionality. Furthermore, the broken symmetry of the Wigner-Seitz cell enabled the plasmonic antenna honeycomb to operate over a broad spectrum, by supporting multiple resonances. A compact formula for the far-zone radiation pattern was derived using the basic principles of classical antenna theory. The proposed plasmonic antenna honeycomb array is particularly attractive for emerging plasmonic and photovoltaic applications that require a unidirectional radiation pattern over a wide spectrum.

Acknowledgments

This work is supported by TUBITAK under projects with the numbers 108T482 and 109T670 and by European Community Marie Curie International Reintegration Grant (MIRG-CT-2007-203690). Kursat Sendur acknowledges partial support from the Turkish Academy of Sciences.